

# A global C-staggered composite model for shallow water equations with latitude-longitude grid and reductions in the polar regions

Genilson S. Lima

Instituto de Matemática e Estatística, Universidade de São Paulo, R. do Matão 1010, São Paulo, 05508-090, Brazil, [genilson@ime.usp.br](mailto:genilson@ime.usp.br)

This preprint is a non-peer-reviewed text submitted to EarthArXiv. This preprint was submitted to the International Journal of Computational Methods in January 2024 for peer review and was accepted in June 2024 after improvements in the text and the inclusion of more numerical examples.

# A global C-staggered composite model for shallow water equations with latitude-longitude grid and reductions in the polar regions

Genilson S. Lima\*

*Instituto de Matemática e Estatística, Universidade de São Paulo, R. do Matão 1010, São Paulo, 05508-090, Brazil*

## ARTICLE INFO

### Keywords:

global reduced grids  
finite differences  
finite volumes  
shallow-water equations  
conservation  
consistency

## ABSTRACT

To develop a numerical method for global geophysical fluids, we usually need to choose a spherical grid and numerical approximations to represent the partial derivative equations. Some alternatives include the use of finite differences or finite volumes with latitude-longitude or reduced grids. Each of these cases has some advantages and also some limitations. This paper presents a comparison between two methods and numerical tests with a composite model using them side by side. The first is a well-known method for latitude-longitude grids that was used from  $75^{\circ}S$  until  $75^{\circ}N$ . The second is a recently developed scheme for reduced grids that was used only in the polar regions. The similarity between these two methods allows a smooth transition in these two regions. Numerical tests with the composite model indicated order 2 of convergence, prevention of grid-imprinting errors, and a combination of the advantages of both schemes. The composite model has numerical properties that may lead to efficient implementations with massive parallel computation.

## 1. Introduction


The behavior of a global model for geophysical fluids depends on the alternatives selected for the continuous equations considered and the discrete operators used to calculate approximations to their solutions [1, 2, 3]. One of the alternatives are methods with Eulerian framework, grid-point orientation, explicit time integration, and local finite-difference or finite-volume expressions [4, 5, 6, 7, 8]. Each method in this group may use a different grid, employ a distinct process to select discrete operators, and present different advantages or limitations.

Latitude-longitude grids have many symmetries and do not need interpolations, but the concentration of points in polar regions may lead to limited computational efficiency. Winninghoff [9] showed that C-staggered grids provide a better representation of the dispersion of gravity waves in explicit methods with approximations with few points. Sadourny [4], Arakawa and Lamb [5] presented explicit schemes for latitude-longitude C-staggered grids with several conservative properties and consistent approximations. However, the concentration of points in the polar regions causes a strong limitation for the size of the time-step allowed by the CFL condition in these explicit methods (Courant-Friedrichs-Lewy condition).

Cubed-sphere and Voronoi grids do not have intense concentration of points and do not need interpolations, but cells with bad alignment of edges may induce stronger errors. Ringler et al. [6] proposed an explicit method with many conservative properties and C-staggered grids without concentration of points, including Voronoi and cubed-sphere grids. Nonetheless, some approximations may become non-consistent (errors may not decrease as the grid resolution increase), and cells with a bad alignment of edges may cause grid-imprinting errors [10, 11].

Reduced grids have many local symmetries and avoid strong concentration of points, but the curvature of latitude lines near polar points may produce larger errors. Shuman [12] and Dey [13] showed that polynomial approximations are not consistent in polar regions of reduced grids. Purser [14] proposed trigonometric discrete operators consistent in these areas. Bénard and Glinon [7] presented a method with non-staggered reduced grids with high consistency order. However, this method does not have conservative properties, and some numerical tests may indicate short wavelength errors in polar regions. Lima and Peixoto [8] proposed a scheme with C-staggered reduced grids, consistent approximations, and conservation of mass. Nonetheless, this method has less conservative characteristics than the schemes presented by Ringler et al. and Sadourny.

The objective of this study is to describe a composite model combining a latitude-longitude method covering a large area of the sphere and a reduced-grid scheme describing only the polar regions. On one hand, Sadourny [4]

 genilson@ime.usp.br (G.S. Lima)  
ORCID(s): 0000-0002-9635-2048 (G.S. Lima)

method is consistent, avoids grid-imprinting, and has several conservative properties (at the cost of a strong limitation in polar regions). On the other hand, the scheme proposed by Lima and Peixoto [8] is consistent, has some conservative properties, avoids grid-imprinting, and allows larger time-steps (at the cost of not preserving some characteristics). As an alternative, we will use this scheme with a reduced grid only where the Sadourny method has its computational limitation. Both methods share several properties in the process used to select their discrete operators. This similarity allows a smooth transition between the two regions.

Section 2 describes the continuous equations, the grid, and the approximations employed by each method. Sections 3 and 4 show numerical tests with the composite model and the final remarks.

## 2. Continuous and discrete equations

### 2.1. Continuous equations

We will consider the vector-invariant form of non-linear shallow water equations on the sphere [5, 15, 6, 8]. This system of equations describes a layer with incompressible fluid moving around a sphere with influence of topography, gravity, and rotation [16, 17].

Coordinates are the moment,  $t \in [t_0, t_{\text{end}}]$ , latitude,  $\varphi \in [-\pi/2, \pi/2]$ , and longitude,  $\lambda \in [-\pi, \pi]$ . Prognostic variables are the layer thickness,  $h(\lambda, \varphi, t)$ , zonal component of velocity,  $u(\lambda, \varphi, t)$ , and meridional component of velocity,  $v(\lambda, \varphi, t)$ .

The continuous solutions have to satisfy given initial conditions,  $h(\lambda, \varphi, t_0)$ ,  $u(\lambda, \varphi, t_0)$ ,  $v(\lambda, \varphi, t_0)$ , and the following system with one Partial Derivative Equation for each prognostic variable,

$$\partial_t h = -\nabla \cdot h\vec{u}, \quad (1)$$

$$\partial_t u = +(\zeta + f)v - \partial_x(K + \Phi), \quad (2)$$

$$\partial_t v = -(\zeta + f)u - \partial_y(K + \Phi). \quad (3)$$

Auxiliary objects are gravity,  $g$ , sphere angular rotation velocity,  $\Omega$ , sphere radius,  $a$ , zonal vector  $\vec{i}(\lambda, \varphi)$ , meridional vector,  $\vec{j}(\lambda, \varphi)$ , velocity vector,  $\vec{u} = u\vec{i} + v\vec{j}$ , altitude direction,  $\vec{k}(\lambda, \varphi)$ , topography,  $b(\lambda, \varphi)$ , horizontal Coriolis function,  $f(\varphi) = 2\Omega \sin(\varphi)$ , relative vorticity,  $\zeta = \vec{k} \cdot \nabla \times \vec{u}$ , kinetic energy,  $K = (u^2 + v^2)/2$ , and geopotential,  $\Phi = g(h + b)$ .

Differential operators are divergence,  $\nabla \cdot \vec{u} = (\partial_\lambda u + \partial_\varphi(v \cos \varphi))/(a \cos \varphi)$ , relative vorticity,  $\vec{k} \cdot \nabla \times \vec{u} = (\partial_\lambda v - \partial_\varphi(u \cos \varphi))/(a \cos \varphi)$ , zonal derivative,  $\partial_x h = \partial_\lambda h/(a \cos \varphi)$ , meridional derivative,  $\partial_y h = \partial_\varphi h/a$ , and partial derivatives,  $\partial_\lambda$ ,  $\partial_\varphi$ , and  $\partial_t$ .

### 2.2. Reduced grids and C-staggering

We will use grids determined by one free parameter related to its resolution and some extra restrictions. The resolution is selected by the number of rows,  $R$ , given as any power of 2 greater than or equal to 64. There are 16 cells around the polar points. The grids have some reduction lines between  $75^\circ$  and the poles and a regular latitude-longitude structure from  $75^\circ S$  until  $75^\circ N$ . With this separation, the latitude-longitude region represents 96.5% of the spherical surface.

Following, we describe the steps used to create these grids. First, we take a regular latitude-longitude grid with  $R$  rows and 16 columns. Next, we split each cell by two in the rows where the ratio between the cell's zonal length and its meridional length is greater than 0.5. Then, this splitting process is repeated in such a way that the maximum number of cells in a row is always less than or equal to  $2R$ , the transition lines have a factor 2 in the number of cells on each side, and there are at least 2 rows between consecutive transition lines.

We used 16 polar cells, and the transition for  $2R$  cells at  $75^\circ$ , but other options could also be selected. Alternatives using a number between 12 and 20 polar cells and the transition for  $2R$  between  $70^\circ$  and  $80^\circ$  provided similar results in the numerical tests.

The discrete variables have a C-staggered positioning at each cell. Discrete thickness,  $h_i(t)$ , are at the latitude-longitude center of each cell,  $\{X_i, i \in \mathcal{I}\}$ . Discrete zonal velocity,  $u_e(t)$ , are at the midpoint of meridional edges,  $\{X_e, e \in \mathcal{E}\}$ . Discrete meridional velocity,  $v_n(t)$ , are at the midpoint of zonal edges,  $\{X_n, n \in \mathcal{N}\}$ . Relative vorticity,  $\zeta_w(t)$ , are at the vertices,  $\{X_w, w \in \mathcal{W}\}$ . Figure 1 show the variable positions for some cells. Black lines indicate the cells around each center point. Red lines represent the dual cells around each vertex.

(a) Points at polar cells

(b) Points near a reduction

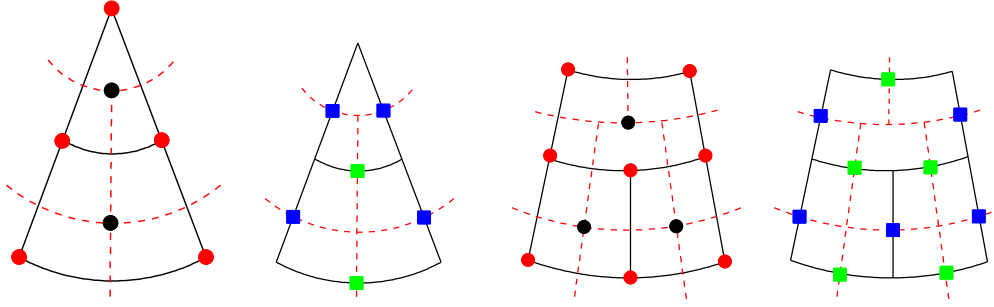


Figure 1: Position of discrete variables near the polar cells (a) or reduction rows (b). Black and red circles represent centroids,  $X_i$ , or vertices,  $X_w$ . Blue and green squares indicate the midpoint of meridional edges,  $X_e$ , or midpoint of zonal edges,  $X_n$ . Black lines represent the edges. Red dashed lines portray the dual cells around each vertex.

### 2.3. Approximations in space

The semi-discrete solutions have to satisfy initial conditions,  $\{h_i(t_0), i \in \mathcal{I}\}$ ,  $\{u_e(t_0), e \in \mathcal{E}\}$ ,  $\{v_n(t_0), n \in \mathcal{N}\}$ , and one Ordinary Differential Equation for each discrete prognostic variable,

$$\partial_t h_i = -[\nabla \cdot h\vec{u}]_i, \quad (4)$$

$$\partial_t u_e = +[(\zeta + f)v]_e - [\partial_x(K + \Phi)]_e, \quad (5)$$

$$\partial_t v_n = -[(\zeta + f)u]_n - [\partial_y(K + \Phi)]_n. \quad (6)$$

These terms between brackets are discrete approximations calculated with variables in a neighborhood of each point.

Following, we will define some auxiliary objects, describe the approximations used by the Sadourny method with conservation of total energy [4], and indicate the adaptations used by the C-staggered trigonometric scheme [8].

The auxiliary measures are the area of each main cell,  $A_i$ , area of each dual cell,  $A_w$ , length of each main edge,  $\Delta x_n$  or  $\Delta y_e$ , and length of each dual edge,  $\Delta x_e$  or  $\Delta y_n$ . Some terms will receive an index with the name of a cardinal direction to indicate the corresponding position in relation to the reference point of each expression. For instance, in the definition of  $\tilde{h}_e$ , the reference point is the edge mid-point  $X_e$ , and  $h_i^{\text{east}}$  is the thickness at the first center point  $X_i$  in the east direction.

#### 1. Divergence and vorticity

Averages of thickness are polynomial interpolations with 2 points. Vorticity and divergence are expressions related to Gauss' theorem using polynomial line quadratures with 1 point. Coriolis function,  $f_w$ , absolute vorticity,  $\xi_w$ , and potential vorticity,  $q_w$ , are calculated at vertices.

$$\tilde{h}_e = 0.5h_i^{\text{east}} + 0.5h_i^{\text{west}}, \quad (7)$$

$$\tilde{h}_n = 0.5h_i^{\text{north}} + 0.5h_i^{\text{south}}, \quad (8)$$

$$\tilde{h}_w = 0.25h_i^{\text{northwest}} + 0.25h_i^{\text{northeast}} + 0.25h_i^{\text{southwest}} + 0.25h_i^{\text{southeast}}, \quad (9)$$

$$[\nabla \cdot h\vec{u}]_i = \frac{1}{A_i} [-(\tilde{h}u\Delta y)_e^{\text{west}} + (\tilde{h}u\Delta y)_e^{\text{east}} + (\tilde{h}v\Delta x)_n^{\text{north}} - (\tilde{h}v\Delta x)_n^{\text{south}}], \quad (10)$$

$$\zeta_w = \frac{1}{A_w} [-(v\Delta y)_n^{\text{west}} + (v\Delta y)_n^{\text{east}} - (u\Delta x)_e^{\text{north}} + (u\Delta x)_e^{\text{south}}], \quad (11)$$

$$\xi_w = \zeta_w + f_w, \quad (12)$$

$$q_w = \xi_w / \tilde{h}_w. \quad (13)$$

The trigonometric scheme uses the same approximations in meridional direction, but zonal interpolations and zonal quadratures are trigonometric expressions with 6 or 5 points, respectively, to achieve consistency [8]. Cells near polar points or reduction rows require some adaptations. For instance, vorticity at the polar point has 16 edges, and divergence near a reduction has 5 edges.

113  
114  
115  
116

## 2. Kinetic energy and directional derivatives

Kinetic energy,  $K_i$ , is a linear combination using the square of normal velocity of each edge. Topography,  $b_i$ , and geopotential,  $\Phi_i$ , are calculated at centers. Directional derivatives are polynomial finite differences with 2 points.

$$K_i = \frac{1}{4A_i} [(u^2 \Delta x \Delta y)_e^{\text{west}} + (u^2 \Delta x \Delta y)_e^{\text{east}} + (v^2 \Delta x \Delta y)_n^{\text{north}} + (v^2 \Delta x \Delta y)_n^{\text{south}}], \quad (14)$$

$$\Phi_i = g(h_i + b_i), \quad (15)$$

$$[\partial_x(K + \Phi)]_e = \frac{1}{\Delta x_e} ((K + \Phi)_i^{\text{east}} - (K + \Phi)_i^{\text{west}}), \quad (16)$$

$$[\partial_y(K + \Phi)]_n = \frac{1}{\Delta y_n} ((K + \Phi)_i^{\text{north}} - (K + \Phi)_i^{\text{south}}). \quad (17)$$

117  
118  
119  
120

The trigonometric method calculates an interpolation of velocity first and then a square. Meridional interpolations and derivatives are polynomial with 2 points. Zonal interpolations and derivatives are trigonometric expressions with 6 or 4 points, respectively. Cells around the polar point use a small adaptation to calculate  $\tilde{v}_i$ . Their meridional interpolation has one  $v_n$  point on each side of the pole.

$$\tilde{u}_i = \text{trigonometric interpolation for } u_e \text{ with 6 points}, \quad (18)$$

$$\tilde{v}_i = 0.5v_n^{\text{north}} + 0.5v_n^{\text{south}}, \quad (19)$$

$$K_i = (\tilde{u}_i^2 + \tilde{v}_i^2)/2, \quad (20)$$

$$[\partial_x(K + \Phi)]_e = \text{trigonometric derivative for } (K_i + \Phi_i) \text{ with 4 points}. \quad (21)$$

121  
122  
123

## 3. Coriolis objects and rotated velocity component

Coriolis terms are linear combinations of products using vorticity, rotated velocity components, and the averages of thickness.

$$\overline{(hv\Delta x)}_w = 0.5(\tilde{h}v\Delta x)_n^{\text{west}} + 0.5(\tilde{h}v\Delta x)_n^{\text{east}}, \quad (22)$$

$$\overline{(hu\Delta y)}_w = 0.5(\tilde{h}u\Delta y)_e^{\text{north}} + 0.5(\tilde{h}u\Delta y)_e^{\text{south}}, \quad (23)$$

$$[\xi v]_e = \frac{1}{2\Delta x_e} [q_w^{\text{north}} \overline{(hv\Delta x)}_w^{\text{north}} + q_w^{\text{south}} \overline{(hv\Delta x)}_w^{\text{south}}], \quad (24)$$

$$[\xi u]_n = \frac{1}{2\Delta y_n} [q_w^{\text{west}} \overline{(hu\Delta y)}_w^{\text{west}} + q_w^{\text{east}} \overline{(hu\Delta y)}_w^{\text{east}}]. \quad (25)$$

124  
125

The trigonometric scheme calculates interpolations first and a product later. Meridional interpolations are polynomial with 2 points, and zonal interpolations are trigonometric with 6 points.

$$\tilde{u}_n = \text{zonal trigonometric interpolation for } u_e \text{ and then a meridional interpolation}, \quad (26)$$

$$\tilde{v}_e = \text{zonal trigonometric interpolation for } v_n \text{ and then a meridional interpolation}, \quad (27)$$

$$\tilde{\xi}_n = \text{trigonometric interpolation for } \xi_w \text{ with 6 points}, \quad (28)$$

$$\tilde{\xi}_e = 0.5\xi_w^{\text{north}} + 0.5\xi_w^{\text{south}}, \quad (29)$$

$$[\xi u]_n = \tilde{\xi}_n \tilde{u}_n, \quad (30)$$

$$[\xi v]_e = \tilde{\xi}_e \tilde{v}_e. \quad (31)$$

126  
127  
128  
129  
130  
131  
132  
133  
134  
135

The composite model uses the expressions from Sadourny in the region from  $75^\circ S$  until  $75^\circ N$ , where the grid has a regular latitude-longitude structure, and the expressions from the C-staggered trigonometric method from  $75^\circ$  until the polar points, where the grid has reduction rows. Considering these definitions, the right side of the system of equations described by 4, 5, and 6 is completely determined. The only unknown objects are the prognostic variables. At the transition between the two schemes, the discrete divergence and vorticity have a small adaptation. The expression calculated with the results of each line integral remains the same, but each line integral is calculated accordingly to the scheme employed at the corresponding edge.

This method is consistent everywhere, has conservation of mass, has global integral of relative vorticity equal to zero, and avoids problems of almost stationary short gravity waves. In the region between  $75^\circ S$  and  $75^\circ N$ , the kinetic energy does not affect the variation of relative vorticity. Total energy is affected only by interactions that may occur

136 in polar regions. Most approximations have symmetrical coefficients. Each cell in the polar regions uses calculations  
137 with 3 points in meridional direction and 7 at zonal direction. In the region with regular grid, the calculations at each  
138 cell use 3 points in each direction.

## 139 2.4. Explicit discrete integration in time

140 Consider a vector-valued function  $Y(t)$  with one coordinate for each prognostic variable  $\{h_i(t), i \in \mathcal{I}\}$ ,  $\{u_e(t), e \in$   
141  $\mathcal{E}\}$ ,  $\{v_n(t), n \in \mathcal{N}\}$ , and a function  $F(Y(t), t)$  representing the corresponding expressions at the right side of the system  
142 of equations given by 4, 5, and 6. Using these objects, the system of Ordinary Differential Equations is written as

$$Y' = F(Y, t), \quad (32)$$

$$Y(t_0) = \text{given}. \quad (33)$$

143 We used a Runge-Kutta method with 3 stages and order 2 to approximate the solution of this system of equations.  
144 Consider a regular set of moments  $t_k = t_0 + k\Delta t$ , and a corresponding set of approximations for  $Y$  at each of these  
145 moments,  $Y_k$ . Each time step is calculated using two intermediate objects,

$$Y^* = Y_k + F(Y_k, t_k)\Delta t/2, \quad (34)$$

$$t^* = t_k + \Delta t/2, \quad (35)$$

$$Y^{**} = Y_k + F(Y^*, t^*)\Delta t/2, \quad (36)$$

$$t^{**} = t_k + \Delta t/2, \quad (37)$$

$$Y_{k+1} = Y_k + F(Y^{**}, t^{**})\Delta t. \quad (38)$$

146 This method for time integration is the same used by Lima and Peixoto [8]. It is an adaptation of the scheme  
147 proposed by Wicker and Skamarock [18]. The adapted version maximizes the allowed size of time steps in the  
148 oscillation problem.

149 The composite model has an option to apply a controlled filter in space after each timestep. The filter parameter is  
150 a number  $\mu \in [0, 1]$ . The filtering is an interpolation with order 2 of consistency that multiplies the shortest wave in  
151 the grid by a factor  $1 - \mu$ . For instance, if  $\mu = 0.1$  then the shortest wave is multiplied by 0.9. The longest waves are  
152 always multiplied by one. In the region from  $75^\circ S$  until  $75^\circ N$ , the transformation uses Shapiro's filter with order 2 in  
153 zonal and meridional directions [19]. In the area from  $75^\circ$  until the polar point, the zonal transformation is replaced  
154 by a trigonometric expression also with order 2 [8]. For any fixed value of  $\mu$ , this filter does not affect the convergence  
155 order and becomes wicker as the grid resolution increases. When the filter is applied, the equation 38 is replaced by  
156 the two following calculations,

$$Y^{***} = Y_k + F(Y^{**}, t^{**})\Delta t, \quad (39)$$

$$Y_{k+1} = \text{Filter}(\mu, Y^{***}). \quad (40)$$

## 157 3. Numerical tests

### 158 3.1. Tests for acumulation of errors

159 This subsection presents two numerical tests over five or six days using the composite method. The first test  
160 considers a steady situation with velocity field across polar regions and large thickness (test case 2 with  $\alpha = \pi/4$  from  
161 cite{WDH+92}). Figure 2 shows thickness, velocity, and thickness error after 5 days of simulation without filtering  
162 and with grid resolution of 256 rows. There is no indication of short-wavelength errors in the transition regions ( $75^\circ S$   
163 and  $75^\circ N$ ) or polar areas in this configuration. When the grid resolution is not very high and the simulation period is  
164 not long, we do not need to use a filter.

165 The second example uses a situation with instability triggered after one week [20, 21]. Figure 3 shows the potential  
166 vorticity after 6 days and the maximum error during the simulated period with filter 0.1. Colors indicate the predicted  
167 results and the black lines represent the reference solution. Level curves in the simulated field have only small  
168 differences when compared to the reference lines. The error stays close to zero for a period and then starts to increase.  
169 When the grid resolution increases, the near-to-zero period lasts longer.

A global C-staggered composite model with latitude-longitude grid and reductions in the polar regions

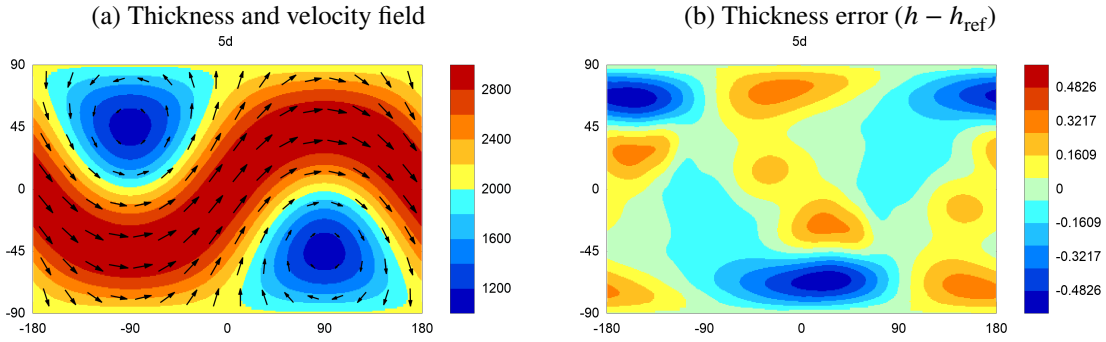


Figure 2: Example considering an equilibrium field with polar wind and large thickness without any filter. Item (a) shows the approximation calculated after 5 days. Item (b) represents the corresponding errors. There is no indication of grid-imprinting errors.

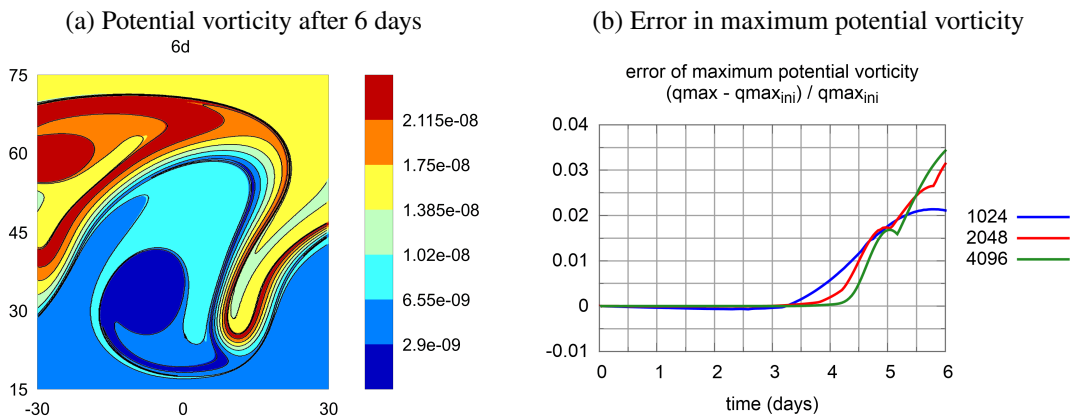


Figure 3: Example describing an instability process with filter  $\mu = 0.1$ . Item (a) uses black lines to indicate the reference solution and colors represent the calculated approximation after 6 days. After 5 days, the level curves are almost equal to the reference solution (not shown). After 6 days, some regions have a small difference. Item (b) shows the variation in the maximum value of potential vorticity. The error increases later when the grid is refined.

### 3.2. Tests for stability and number of calculations

This subsection describes the results obtained with two tests with 30 days of simulation, and compares the number of calculations for the composite model or the two methods alone. The first test is the steady example with velocity across polar regions and large thickness [15]. Figure 4 indicates the thickness error during the simulation for different grid resolutions in the situation (a) without any filter or (b) with filter  $\mu = 0.1$ . Grid resolution increases with factor 2 at each consecutive curve. Marks in the vertical axis represent a multiplication with factor 4. Without a filter, the error decays with order 2 in the beginning of the simulation, but there is an instability process triggered sooner as the grid resolution increases. With filter  $\mu = 0.1$ , the error decays with order 2 and the instability is prevented.

The second test uses a low-resolution grid with an almost steady situation [8]. The initial pulse is represented by 10 grid rows. Figure 5 shows the simulated field after 30 days in the situation (b) without filter or (b) with filter  $\mu = 0.1$ . Without filter, the pulse amplitude is almost preserved. With a filter, the amplitude decayed by a half. There is no indication of decomposition creating strong gravity waves.

The third test compares the number of calculations in the composite model and in the situation when each of its two methods is used alone in the entire sphere. Figure 6 shows (a) the total processing time and (b) the average time for each time step at each grid cell considering a simulation with one single processing core. Sadourny method [4] uses a complete latitude-longitude grid, has slope 4 in the total processing time for different grid resolutions, and the average cost at each cell is smaller. The trigonometric C-staggered method [8] uses a reduced grid, has slope 3 in the total processing time, and the average cost at each cell is larger. The composite model uses reductions only above 75

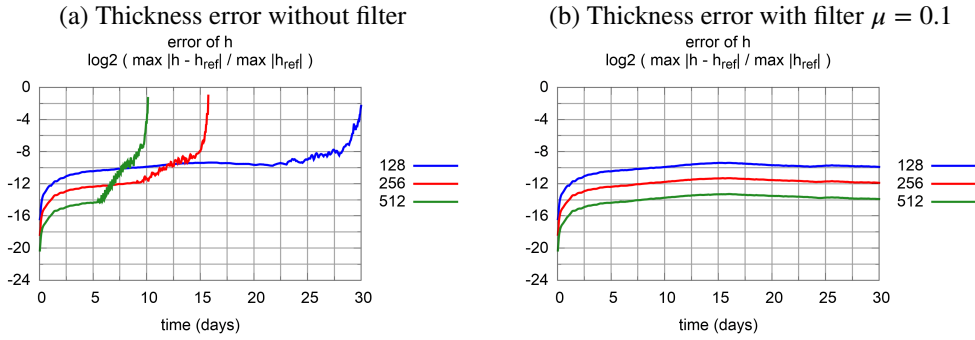


Figure 4: Example with polar wind and large thickness without any filter (a) or with filter  $\mu = 0.1$  (b). Each curve indicates the error with a different grid. Without filtering, the method has non-linear instability. With the controlled dumping, the model has second order of convergence.

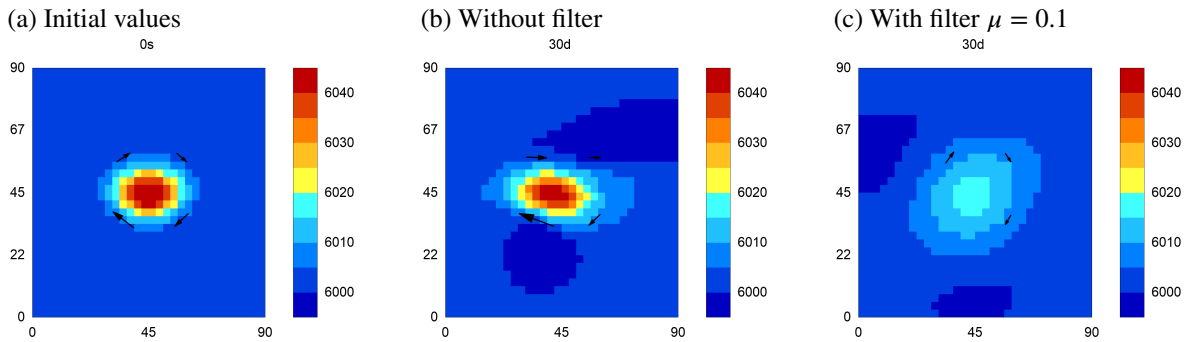


Figure 5: Example considering a constant field with low resolution. Without a filter, the amplitude is almost preserved after 30 days (b). With the limited dumping, the signal is partially preserved, but the amplitude is smaller (c). In both situations, there is no indication of deterioration as strong gravity waves.

188 degrees, has slope 3 in the total processing time, and the average cost at each cell is similar to the cost of the Sadourny  
 189 method.

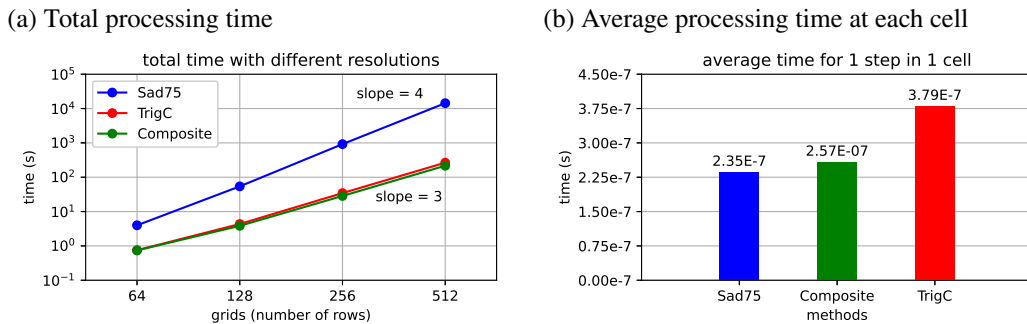


Figure 6: Comparison of the number of calculations used by the Sadourny method (Sad75), the trigonometric scheme with C-staggered reduced grid (TrigC) and the model using these two schemes side by side (Composite). The composite model has a total number of calculations a little smaller than the trigonometric method and an average number of calculations for each step in each cell a little larger than the Sadourny scheme.



## 4. Final remarks

This study compared two numerical methods with different grids and proposed a composite model employing each scheme in a region on the sphere. Sadourny method is used in a regular latitude-longitude grid region from  $75^{\circ}S$  until  $75^{\circ}N$ , covering more than 95% of the spherical surface. The trigonometric C-staggered scheme is employed in a reduced grid from  $75^{\circ}$  until the polar points.

The composite model uses grid-point finite-difference or finite-volume approximations, explicit second-order time integration, local approximations with second order of consistency (error of local approximations decreases with order 2 when the grid resolution increases), has a good representation of gravity waves propagation, conserves total mass, has a structure to cancel artificial influences in the total energy in the latitude-longitude region, avoids grid imprinting errors, allows the use of a consistent filter to prevent short-wavelength instability, and presented second order of convergence in the numerical tests.

Future steps in this subject may include the implementation of this composite model with distributed memory, tests with higher resolution latitude-longitude grid in local regions, and alternatives for 3-dimensional global hydrostatic models.

## Declaration of competing interest

The authors declare that they have no known competing financial interests or personal relationships that could have appeared to influence the work reported in this paper.

## References

- [1] A. A. White, A view of the equations of meteorological dynamics and various approximations, *Analytical Methods and Numerical Models* 1 (2002) 1–100.
- [2] D. L. Williamson, The evolution of dynamical cores for global atmospheric models, *Journal of the Meteorological Society of Japan* 85 (2007) 241–269.
- [3] A. Staniforth, J. Thuburn, Horizontal grids for global weather and climate prediction models: A review, *Quarterly Journal of the Royal Meteorological Society* 138 (2012) 1–26.
- [4] R. Sadourny, The dynamics of finite-difference models of the shallow-water equations, *Journal of Atmospheric Sciences* 32 (1975) 680–689.
- [5] A. Arakawa, V. R. Lamb, A potential enstrophy and energy conserving scheme for the shallow water equations, *Monthly Weather Review* 109 (1981) 18–36.
- [6] T. D. Ringler, J. Thuburn, J. B. Klemp, W. C. Skamarock, A unified approach to energy conservation and potential vorticity dynamics for arbitrarily-structured C-grids, *Journal of Computational Physics* 229 (2010) 3065–3090.
- [7] P. Bénard, M. R. Glinton, Circumventing the pole problem of reduced lat–lon grids with local schemes. Part I: Analysis and model formulation, *Quarterly Journal of the Royal Meteorological Society* 145 (2019) 1377–1391.
- [8] G. S. Lima, P. S. Peixoto, A consistent mass-conserving c-staggered method for shallow water equations on global reduced grids, *Journal of Computational Physics* 473 (2023) 111741.
- [9] F. J. Winninghoff, On the adjustment towards a geostrophic balance in a simple primitive equation model with application to the problems and objective analysis, Ph.D. thesis, Ph. D. thesis, University of California, 1968.
- [10] P. S. Peixoto, S. R. M. Barros, Analysis of grid imprinting on geodesic spherical icosahedral grids, *Journal of Computational Physics* 237 (2013) 61–78.
- [11] H. Weller, J. Thuburn, C. J. Cotter, Computational modes and grid imprinting on five quasi-uniform spherical C grids, *Monthly Weather Review* 140 (2012) 2734–2755.
- [12] F. G. Shuman, On certain truncation errors associated with spherical coordinates, *Journal of Applied Meteorology* 9 (1970) 564–570.
- [13] C. H. Dey, A note on global forecasting with the Kurihara grid, *Monthly Weather Review* 97 (1969) 597–601.
- [14] R. J. Purser, Accurate numerical differencing near a polar singularity of a skipped grid, *Monthly Weather Review* 116 (1988) 1067–1076.
- [15] D. L. Williamson, J. B. Drake, J. J. Hack, R. Jakob, P. N. Swarztrauber, A standard test set for numerical approximations to the shallow water equations in spherical geometry, *Journal of Computational Physics* 102 (1992) 211–224.
- [16] J. Pedlosky, *Geophysical fluid dynamics*, volume 710, Springer, 1987.
- [17] G. K. Vallis, *Atmospheric and oceanic fluid dynamics*, Cambridge University Press, 2006.
- [18] L. J. Wicker, W. C. Skamarock, Time-splitting methods for elastic models using forward time schemes, *Monthly Weather Review* 130 (2002) 2088–2097.
- [19] R. Shapiro, Linear filtering, *Mathematics of Computation* 29 (1975) 1094–1097.
- [20] J. Galewsky, R. K. Scott, L. M. Polvani, An initial-value problem for testing numerical models of the global shallow-water equations, *Tellus A: Dynamic Meteorology and Oceanography* 56 (2004) 429–440.
- [21] R. K. Scott, L. M. Harris, L. M. Polvani, A test case for the inviscid shallow-water equations on the sphere, *Quarterly Journal of the Royal Meteorological Society* 142 (2016) 488–495.